Progress report on 2015 SCEC proposal: Multi-scale stress and strain-rate model analysis for southern California

Thorsten W. Becker

October 22, 2016

Objective

SCEC IV was committed to the development of a Community Stress Model (CSM), and such an effort speaks to core problems of earthquake mechanics; how faults are loaded, and how the stress changes due to individual ruptures affect the overall stress state of the system.

For this particular, SCEC CSM related project, we proposed to use and expand the wavelet-based analysis of *Tape et al.* (2009) to understand the degree of agreement between different representations of stress and stressing-rate in southern California. As a baseline, we also suggested the development of a *Kostrov* (1974) summation of the *Yang et al.* (2012) focal mechanism catalog. No such model of strain-rate (or stress, if interpreted such in the case of normalized summations) had been submitted to the SCEC CSM previously. Such a model would also be useful to compare results with *Michael* (1984) type stress inversions (cf. *McKenzie*, 1969; *Becker et al.*, 2005).

We made good progress on the latter model building, performed some initial, wavelength-dependent analysis based on Fourier filtering, but still have to complete the wavelet based analysis. We report on project-related efforts below.

Progress

Kostrov summation model

Following the approach outlined in detail in *Platt and Becker* (2010), we computed *Kostrov* (1974) summations of normalized moment tensors as inferred from focal mechanisms for southern California. When using full moment tensors, such a summation is a direct representation of the co-seismic strain release in the region during the time period of summation. When normalized moment tensors are summed, such analysis can represent the typical deformation style (e.g. *Bailey et al.*, 2009; *Platt and Becker*, 2010). Strain need not be aligned with stress in the presence of

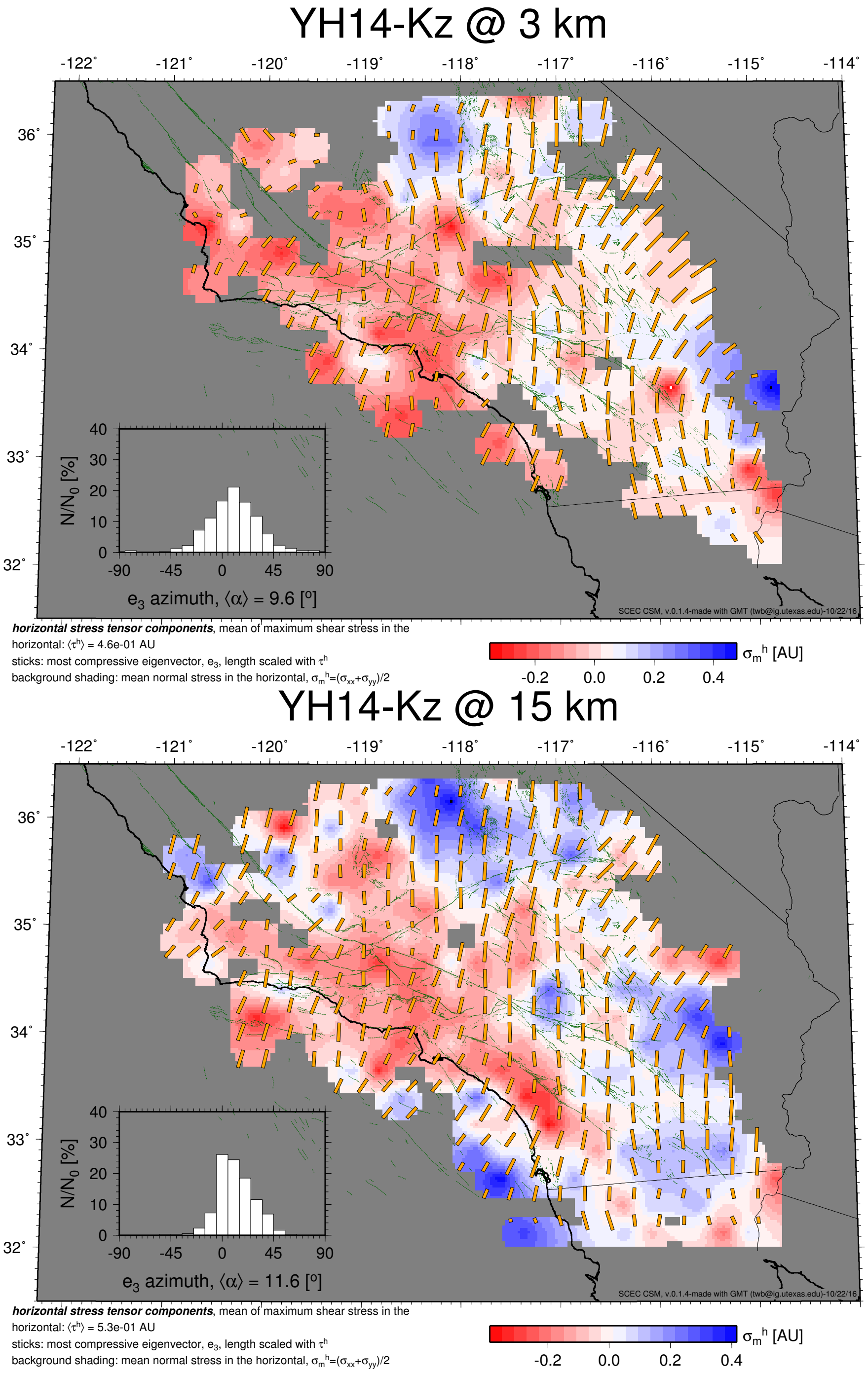

Figure 1: Horizontal "stress" component of the new *YH14-K* model, at shallow and larger depth layers, based on *Kostrov* (1974) summation of the 2014 update of the *Yang et al.* (2012) focal mechanisms. SCEC-CSM style plot (*Yu et al.*, 2013) for the horizontal tensor components only, stick orientations showing major compressive axes, background shading mean normal stress

frictional slip on fault planes (e.g. *McKenzie*, 1969; *Michael*, 1984). However, empirically, the deviations between stress inferred by *Michael* (1984) type inversion and Kostrov strain for southern California appears small (*Becker et al.*, 2005).

As focal mechanism data, we use the 2014 update of the *Yang et al.* (2012) catalog (http://scedc.caltech.edu/research-tools/alt-2011-yang-hauksson-shearer.html, accessed 2016). We sum the normalized moment tensors inferred from the focal mechanisms in $0.25° \times 0.25°$ bins, and compute two versions of the model: *YH14-K*, which uses all events in the bin, and *YH14-Kz*, which splits shallow and deep events into a two layer representation using 8 km (the approximate median of the event depths in the catalog) as the boundary. We explored time-dependent summation of the catalog, but found variations in deformation style to be minor (cf. *Yang et al.*, 2012) and use the full temporal catalog extent. Bins with one focal mechanism are allowed, but median numbers for the combined, shallow, and deep summations are 8, 6, and 5, respectively.

Model *YH14-Kz* is shown for the two layers in Figure 1. “Stress” (or strain release) orientations are similar in the shallow and deeper crust (cf. *Yang and Hauksson*, 2013). However, major compressive, axes tend to be oriented more easterly at depth, with mean compressive azimuth of 12° vs. 10°. It seems promising to analyze such variations further in the context of seismic anisotropy and deformation models.

YH14-K was submitted to the SCEC CSM model repository (*Yu et al.*, 2013) and can now be analyzed along-side the other models at https://sceczero.usc.edu/projects/CSM/. It can be considered a simple reference to compare the more elaborate models to, and might be a candidate for a model of type 2A: “Kostrov summation of co-seismic strain-release based”, as per the CSM web page.

SCEC CSM validation and web page updates

Project funding also allowed working with John Yu of USC to keep the SCEC CSM web page up to date (cf. *Yu et al.*, 2013). For exmaple, Michelle Cooke (U Mass Amherst) submitted several new models during the project duration, and the incorporation of new models into the plotting scripts and web interface is regrettably still somewhat work intensive.

Funding also allowed comparative analysis of different models. The various inter-model comparison maps are, of course, available on the CSM web page (see, e.g., https://sceczero.usc.edu/projects/CSM/stress?test=tdot for inter-model comparison matrices). However, we have also begun to explore other ways of validating, or scoring, different models. Figure 2 shows one way of expressing overall model performance by means of comparison with the World Stress Map (WSM; *Zoback*, 1992; *Heidbach et al.*, 2008) constraints. SCEC CSM models typically cover $\approx 85\%$ to 100% of the WSM constraints (see symbol size in Figure 2). Out of those constraints sampled by the CSM, the majority of the 2008 WSM release constraints are based on focal mechanisms, corresponding to $\approx 75\%$ in the southern California, SCEC CSM domain. This means that strong circularity is introduced if the WSM is used to “test” CSM models, most of which also use focal mechanism information. However, we note that those are typically from local catalogs rather than the Harvard/Global CMT solutions (only complete down to $M \approx 5$) as used the WSM.

The breakdown into constraints from the WSM with and without focal mechanisms in Figure 2 therefore expectedly shows smaller RMS deviations for focal mechanisms, or the complete

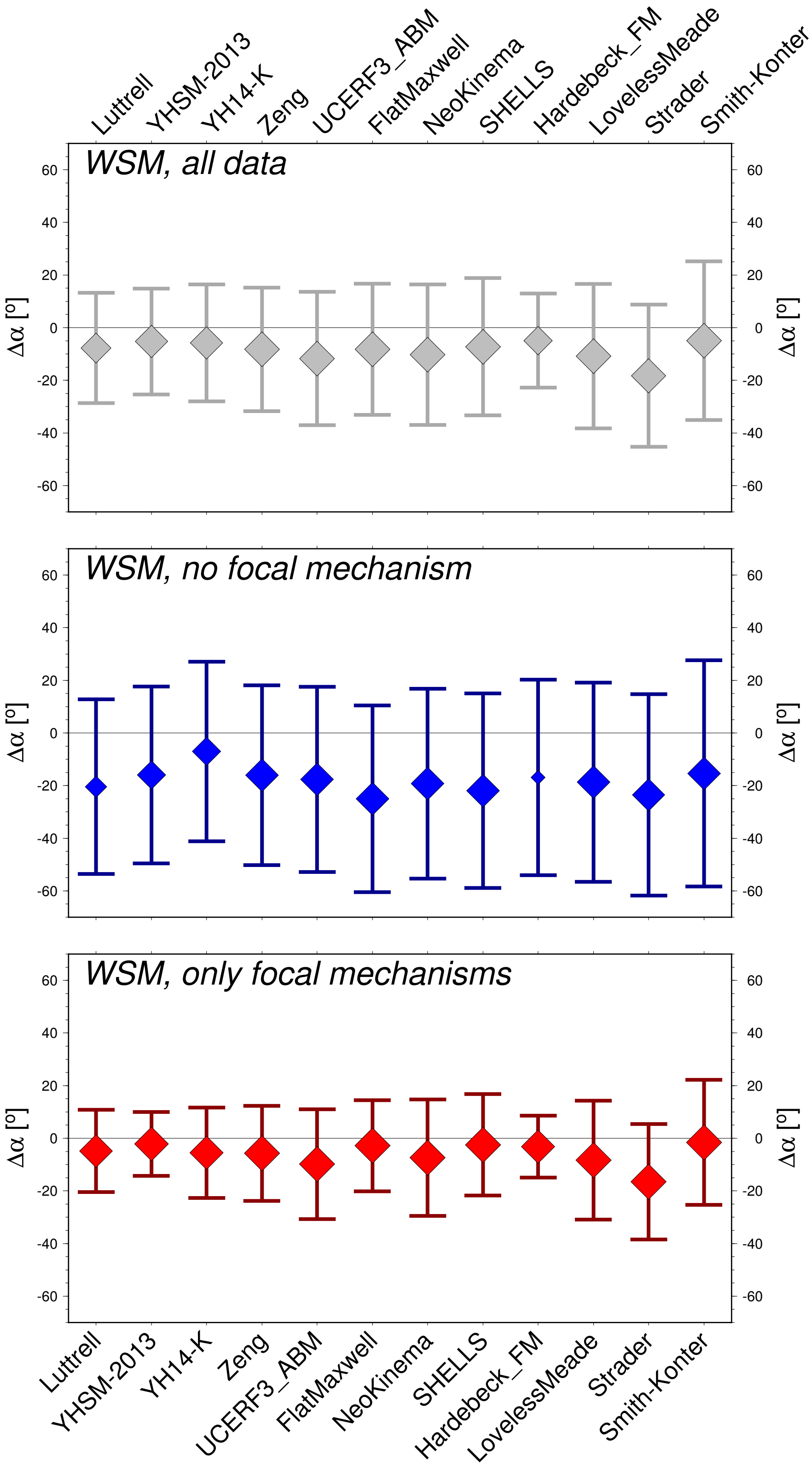

Figure 2: SCEC Community Stress Model validation results: Mean (diamonds) and RMS (error bars) angular deviation, $\Delta\alpha$, of major compressive axes in the horizontal with World Stress Map (WSM; *Heidbach et al.*, 2008) constraints for southern California (region as in Figure 1). Plots show CSM model performance when all constraints (top), only those which do not rely on focal mechanisms (center), and only those using focal mechanism (bottom) are used. Symbol sizes are scaled by the fraction of each set of WSM constraints sampled by the respective CSM stress model, and WSM focal mechanism constraints make up $\approx 75\%$ of the total. Stress and stressing-rate models are sorted in order decreasing RMS deviation for the central plot (model names as in the SCEC CSM, see there for references, cf. *Yu et al.*, 2013).

WSM constraints, than for those few WSM constraints which are not from seismicity (mainly from borehole breakouts, and some tectonic indicators).

Considering the focal mechanism WSM, the *Hardebeck_FM* model is closest to the WSM in terms of mean orientation and smallest RMS. *Hardebeck_FM* is a *Hardebeck and Michael* (2006) stress inversion of the *Yang et al.* (2012) catalog, in an approach very similar to *YHSM-2013*, the CSM candidate release by *Yang and Hauksson* (2013). It is interesting that the RMS deviations of *Hardebeck_FM* are smaller than for *YHSM-2013* or our Kostrov summation *YH14-K* which might have been expected to be closest to the WSM interpretation of focal mechanisms. This may indicate a difference between strain-release in large (CMT) and smaller, regional earthquakes, perhaps better captured by stress inversions.

All SCEC CSM models have significantly larger scatter from the non focal mechanism constraints of the WSM (Figure 2). *Luttrell* (*Luttrell et al.*, 2012) is the model with the smallest RMS deviation from the "borehole" data, followed by *YHSM-2013* and *YH14-K* with likely insignificantly different degree of variance reduction. Unlike for the focal mechanisms, the mean angular deviation is significantly different from zero, indicating that the CSM models are trending with an azimuth $\approx 20^\circ$ more westerly than the WSM borehole constraints. The only model for which this is not the case is our Kostrov summation, *YH14-K*, whose average is very close to the WSM compressive axes constraints. However, even *YH14-K* has quite large RMS scatter from that mean.

These results are interesting, as they may imply a physical reason for the misfit with borehole and other constraints from the WSM. They would also imply that the SCEC CSM models have poor predictive power when it comes to explaining constraints that did not go into the model construction itself. However, firm conclusions should await the reanalysis of borehole data for the southern California region, and a more careful quality control on the WSM constraints.

Wavelength-dependent analysis

Figure 3 shows a comparison between the *Yang and Hauksson* (2013) inversion of the *Yang et al.* (2012) catalog and our Kostrov summation of a slightly updated version of that catalog. As discussed above, and anticipated given the results of *Becker et al.* (2005), the "stress" orientations are indeed quite similar. This may imply the alignment of coseismic strain-release and inferred stress, implying a minor role of friction, or, rather, an overall effect of homogenization given that friction values may be variable (cf. *Hardebeck*, 2006).

There are regional exceptions such as in the Eastern California Shear Zone and at the southern end of the Carrizo segment. Regional misfit patterns are overall consistent when the full tensor product rather than the horizontal projection of the major axes are considered. Howver, the deviations are expectedly larger, leading to $\langle x \rangle \approx 0.76$ compared to the 0.97 of Figure 3 (unity being perfect match).

If we compare the deformation style inferred from the normalized Kostrov summation of *YH14-K* with geodetically derived stressing rate, such as the UCERF3 (*Field et al.*, 2014) average block model, *UCERF3_ABM*, the match is slightly reduced compared to Figure 3, but still quite high at mean dot product values of $\langle x \rangle \approx 0.92$. Aspects of the spatial patterns of deviations are similar, too (e.g., Figure 3), such as in the southern part of the Carrizo segment. This may indicate a physically significant origin of mismatch between seismic strain release and inferred stress or

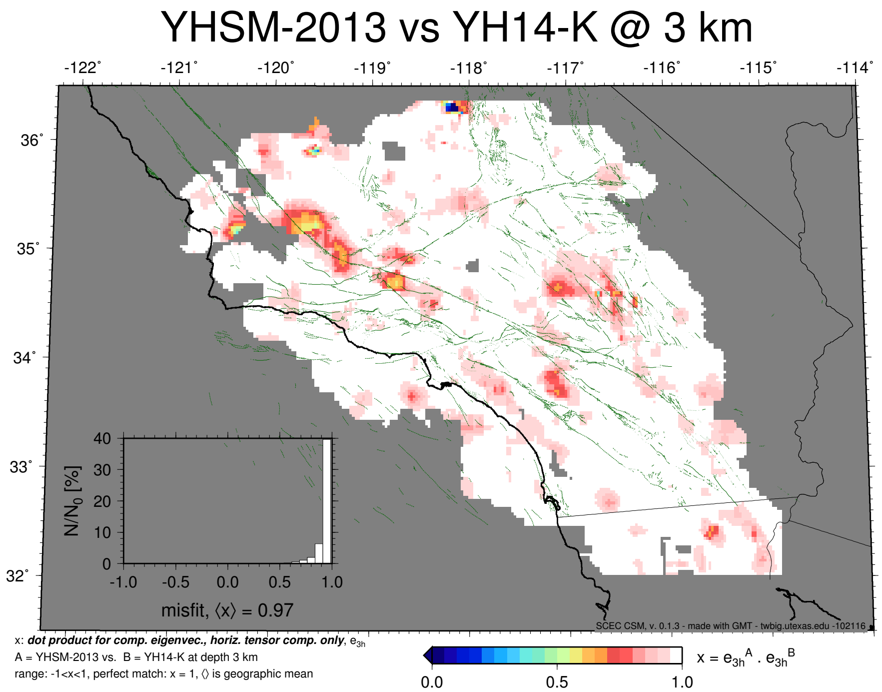

Figure 3: Deviation between the SCEC CSM candidate release, *YHSM-2013* by *Yang and Hauksson* (2013), and our Kostrov summation, *YH14-K*, in terms of dot product between horizontal projection of the major compressive axes, plotted in the SCEC CSM style (*Yu et al.*, 2013).

geodetic stressing rate. However, overall the conclusions of *Becker et al.* (2005) are confirmed by this analysis; geodetic strain-rates and "stress", however it is measured, align.

Figure 4 represents an initial attempt to quantify the wavelength character of deviations. We show example model comparisons where the mean dot product misfit and the RMS variations are computed after both models to be compared are low-pass filtered for different cut-off wavelengths, λ, using the GMT *grdfft* (*Wessel and Smith*, 1995) Fourier based approach of *Becker et al.* (2014).

The top row (Figures 4a-c) explores the match between the *Yang et al.* (2012) catalog based Kostrov summations and the *Hardebeck and Michael* (2006) style stress inversions of *Yang and Hauksson* (2013) and J. Hardebeck (https://sceczero.usc.edu/projects/CSM/model_metadata?type=stress&model=Hardebeck_FM). The two stress inversions are expectedly very similar, even at short wavelengths, and the Kostrov summation is closer to Hardebeck's inversion than that of *Yang and Hauksson* (2013). This indicates that even the same inversion strategy and identical input data can lead to noticeably different results given remaining choices such as to spatial model discretization and smoothing (*Hardebeck and Michael*, 2004; *Hardebeck*, 2006). However, once each model is smoothed such that signals shorter than $\sim$ 200 km are suppressed, the match of the three models is near perfect. The resulting model is, admittedly, likely too coarse to be useful for much besides the most general assessments of the lithosphere's deformation state in the region.

The center row (Figures 4d-f) compares the focal mechanism based inferences of stress with the stressing rate of the average UCERF block model, *UCERF3_ABM*, as in Figure 3. As partially discussed throughout the CSM project process (e.g. *Hardebeck et al.*, 2013), there are significant differences between the two types of models. As we show newly here, those differences persist at all but the longest wavelengths, where $\lambda \sim$ 500 km is a nearly regionally constant model. The rollover toward greater similarity happens at $\approx$ 100 km for *YH14-K* but only at $\approx$ 300 km for

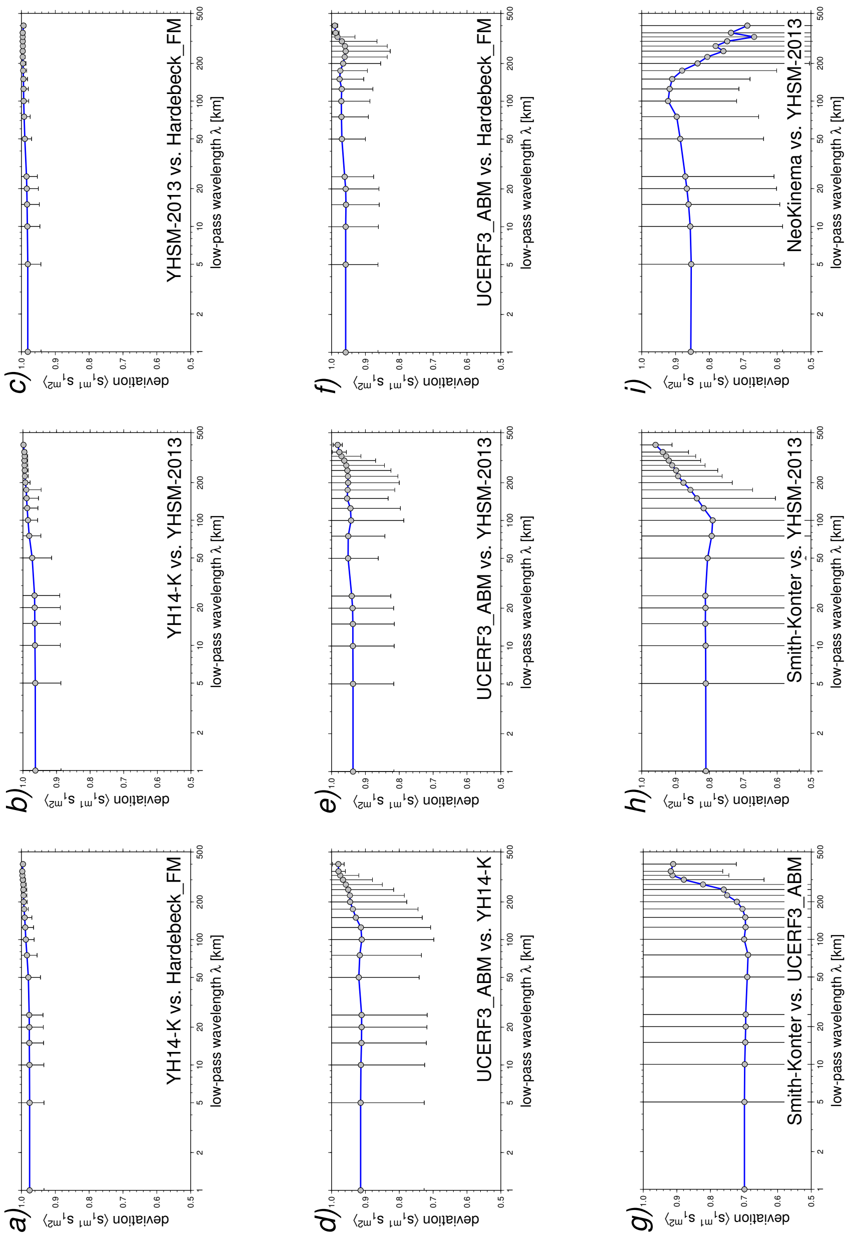

Figure 4: Wavelength-dependent deviation between models (measured in terms of normalized dot product of the horizontal major compressive axes, as in Figure 3). Dots show median values, error bars RMS variations similar to Figure 2. A low-pass spatial filter is applied with wavelength, λ, on the *x*-axes (cf. *Becker et al.*, 2014, for details), larger smoothing is to the right. SCEC CSM model names (*Yu et al.*, 2013) indicated in each subplot.

Hardebeck_FM.

Figure 4g compares the fault-centric, geodesy based stressing-rate model *Smith-Konter* (cf. *Smith and Sandwell*, 2003; *Tong et al.*, 2014) with the *UCERF3_ABM*, indicating that there are large differences in the inferred stressing-rate, and that those are not reconcilable by smoothing. The same is true when comparing with stress from *YHSM-2013* (Figure 4h), although the deviation is, intriguingly, smaller than for the similarly geodesy based *UCERF3_ABM*. Lastly, *NeoKinema* (https://sceczero.usc.edu/projects/CSM/model_metadata?type=stressing_rate&model=NeoKinema, see the appendix of *Liu and Gurnis*, 2008) is characterized by deviations from other models (Figure 4i) that indicate that there are strong differences at the longest wavelengths, while the shorter scale features are more similar.

Next steps

A wavelet analysis of the deviations, and an individual model coherence analysis, of the length-scales over which different CSM stress and stressing-rate models, and other sets of deformation indicators such as seismic anisotropy in the mantle and crust, should still be attempted. Such analysis will also have to consider how much of the wavelength-dependence is merely due to modeling assumptions (e.g. parameterization), and which aspects of the behavior may be meaningful to explore in terms of physical causes.

We hope to be able to complete this project during an ongoing collaboration with Adrian Borsa (UCSD) on GPS verticals (formerly also SCEC, and now NASA funded).

References

Bailey, I. W., T. W. Becker, and Y. Ben-Zion (2009), Patterns of co-seismic strain computed from southern California focal mechanisms, *Geophys. J. Int.*, *177*, 1015–1036.

Becker, T. W., J. L. Hardebeck, and G. Anderson (2005), Constraints on fault slip rates of the southern California plate boundary from GPS velocity and stress inversions, *Geophys. J. Int.*, *160*, 634–650.

Becker, T. W., C. Faccenna, E. D. Humphreys, A. R. Lowry, and M. S. Miller (2014), Static and dynamic support of western U.S. topography, *Earth Planet. Sci. Lett.*, *402*, 234–246.

Field, E. H., et al. (2014), Uniform california earthquake rupture forecast version 3 (ucerf3) the time-independent model, *Bull. Seismol. Soc. Am.*, *104*, 1122–1180.

Hardebeck, J., B. Aagaard, T. W. Becker, B. Shaw, and J. Shaw (2013), Workshop Report for *Community Stress Model (CSM) 2012 Workshop*, SCEC Award 12114, Available online at http://sceczero.usc.edu/dashboard/darel/search/product?pid=32, accessed 10/2013.

Hardebeck, J. L. (2006), Homogeneity of small-scale earthquake faulting, stress and fault strength, *Bull. Seismol. Soc. Am.*, *96*, 1675–1688.

Hardebeck, J. L., and A. J. Michael (2004), Stress orientations at intermediate angles to the San Andreas Fault, California, *J. Geophys. Res.*, *109*, doi:10.1029/2004JB003239.

Hardebeck, J. L., and A. J. Michael (2006), Damped regional-scale stress inversions: Methodology and examples for southern California and the Coalinga aftershock sequence, *J. Geophys. Res.*, *111*(B11310), doi:10.1029/2005JB004144.

Heidbach, O., M. Tingay, A. Barth, J. Reinecker, D. Kurfeß, and B. Müller (2008), The World Stress Map database release 2008, doi:10.1594/GFZ.WSM.Rel2008.

Kostrov, B. V. (1974), Seismic moment and energy of earthquakes and seismic flow of rock, *Phys. Solid Earth*, *1*, 23–40.

Liu, L., and M. Gurnis (2008), Simultaneous inversion of mantle properties and initial conditions using an adjoint of mantle convection, *J. Geophys. Res.*, *113*(B08405), doi:10.1029/2008JB005594.

Luttrell, K., B. Smith-Konter, and D. Sandwell (2012), Investigating absolute stress in southern California: How well do stress models of compensated topography and fault loading match earthquake focal mechanisms?, in *Southern California Earthquake Center Annual Meeting 2012 Program*, pp. 121–122, available online at http://www.scec.org/meetings/2012am/SCECProceedingsXXII_2012.pdf, accessed 10/2013.

McKenzie, D. P. (1969), The relation between fault plane solutions for earthquakes and the directions of the principal stresses, *Bull. Seismol. Soc. Am.*, *59*, 591–601.

Michael, A. J. (1984), Determination of stress from slip data; faults and folds, *J. Geophys. Res.*, *89*, 11,517–11,526.

Platt, J. P., and T. W. Becker (2010), Where is the real transform boundary in California?, *Geochem., Geophys., Geosys.*, *11*(Q06013), doi:10.1029/2010GC003060.

Smith, B. R., and D. Sandwell (2003), Coulomb stress accumulation along the San Andreas fault system, *J. Geophys. Res.*, *108*(2296), doi:10.1029/2002JB002136.

Tape, C., P. Musé, M. Simons, D. Dong, and F. Webb (2009), Multiscale estimation of GPS velocity fields, *Geophys. J. Int.*, *179*, 945–971.

Tong, X., B. Smith-Konter, and D. T. Sandwell (2014), Is there a discrepancy between geological and geodetic slip rates along the San Andreas Fault System?, *J. Geophys. Res.*, pp. 2518–2538, doi:10.1002/2013JB010765.

Wessel, P., and W. H. F. Smith (1995), New version of the Generic Mapping Tools released, *Eos Trans. AGU*, *76*, 329.

Yang, W., and E. Hauksson (2013), The tectonic crustal stress field and style of faulting along the Pacific North America Plate boundary in Southern California, *Geophys. J. Int.*, *194*, 100–117.

Yang, W., E. Hauksson, and P. Shearer (2012), Computing a large refined catalog of focal mechanisms for southern California (1981 – 2010): Temporal stability of the style of faulting, *Bull. Seismol. Soc. Am.*, *102*, 1179–1194.

Yu, J., T. W. Becker, J. Hardebeck, and SCEC CSM working group (2013), The SCEC Community Stress Model web site – v.0.1, in *Annual Meeting 2014, Proceedings Volume XXIII*, p. 159, Southern California Earthquake Center, Los Angeles, CA, available online at http://www.scec.org/meetings/2013am/SCEC2013Proceedings.pdf, also see http://sceczero.usc.edu/projects/CSM, both accessed 10/2014.

Zoback, M. L. (1992), First- and second-order patterns of stress in the lithosphere: The World Stress Map project, *J. Geophys. Res.*, *97*, 11,703–11,728.